Sp-47
6345
P-9

TDA Progress Report 42-123

November 15, 1995

# Wind Gust Models Derived from Field Data

W. Gawronski

Communications Ground Systems Section

*Wind data measured during a field experiment were used to verify the analytical model of wind gusts. Good coincidence was observed; the only discrepancy occurred for the azimuth error in the front and back winds, where the simulated errors were smaller than the measured ones. This happened because of the assumption of the spatial coherence of the wind gust model, which generated a symmetric antenna load and, in consequence, a low azimuth servo error. This result indicates a need for upgrading the wind gust model to a spatially incoherent one that will reflect the real gusts in a more accurate manner.*

*In order to design a controller with wind disturbance rejection properties, the wind disturbance should be known at the input to the antenna rate loop model. The second task, therefore, consists of developing a digital filter that simulates the wind gusts at the antenna rate input. This filter matches the spectrum of the measured servo errors. In this scenario, the wind gusts are generated by introducing white noise to the filter input.*

## I. Introduction

The steady-state wind pressure distribution on scaled antenna models was measured during wind tunnel experiments,[1,2,3] and their validity for actual field antennas was unknown. Wind field data collected recently at the DSS-13 antenna were used to evaluate the accuracy of the steady wind pressure measured in the wind tunnel [2]. A similar evaluation can be done for the time-varying part (gusts) of the wind.

The wind gust analytical model, as developed in [1], is used to simulate the pointing errors of the DSN antennas. The model was developed using the wind tunnel data (as in Footnotes 1 through 3) and the Davenport spectra, but its accuracy was unverified. In this article, the wind measurements of servo errors obtained on January 24, 1994, at the DSS-13 antenna site, c.f. [2], were compared with the simulated servo errors. In most cases, the comparison shows satisfactory coincidence between the measured and the simulated data.

---

[1] N. L. Fox and B. Layman, Jr., "Preliminary Report on Paraboloidal Reflector Antenna Wind Tunnel Tests," JPL Interoffice Memorandum CP-3 (internal document), Jet Propulsion Laboratory, Pasadena, California, 1962.

[2] N. L. Fox, "Load Distributions on the Surface of Paraboloidal Reflector Antennas," JPL Interoffice Memorandum CP-4 (internal document), Jet Propulsion Laboratory, Pasadena, California, 1962.

[3] R. B. Blaylock, "Aerodynamic Coefficients for a Model of a Paraboloidal Reflector Directional Antenna Proposed for a JPL Advanced Antenna System," JPL Interoffice Memorandum CP-6 (internal document), Jet Propulsion Laboratory, Pasadena, California, 1964.

Recently, the linear quadratic Gaussian (LQG) controller for the DSS-13 antenna was designed and tested (see [4]). This model-based controller used the identified DSS-13 antenna model based on field experiments [3]. This antenna model does not include the wind disturbances, which are necessary for the design of an improved LQG controller with wind disturbance rejection properties. For this purpose, the wind-measured data were used to create the wind disturbance input into the antenna rate-loop model and will serve as a base for the design of an improved controller with wind disturbance rejection properties.

## II. Evaluation of the Analytical Model

In the field experiment, the servo errors due to wind gusts were measured for the elevation angles from 11 to 89 deg and for the the yaw angles (antenna azimuth position with respect to the wind direction) from 0 to 360 deg. The servo errors from the analytical model are available for elevation angles of 60 and 90 deg and for yaw angles of 0 (front wind), 90 (side wind), and 180 deg (back wind). The results are obtained in the form of the standard deviations of the measured servo error, typically of the length of 8000 samples collected at a sampling time of 0.02 s. The results of field measurements and simulations are shown in Figs. 1 through 4, where "x" denotes field data and "o" denotes the analytical results. For the elevation servo error measurements, there were multiple collections of the field data for each elevation position. Thus, in this case, the maximal and minimal root-mean-square sums of the measured error are plotted with the gray area between them (see Figs. 1 through 3). For the azimuth errors, there was one collection of data, so the field errors do not include the gray area.

The elevation servo error plots indicate that the analytical error lies within the gray area of the min–max measurements, while the results of the azimuth error show very close relationship between the measured and simulated standard deviations of the servo error for the side wind and a discrepancy for the front and back winds. In the latter case, the analysis underestimates the error because of the symmetry
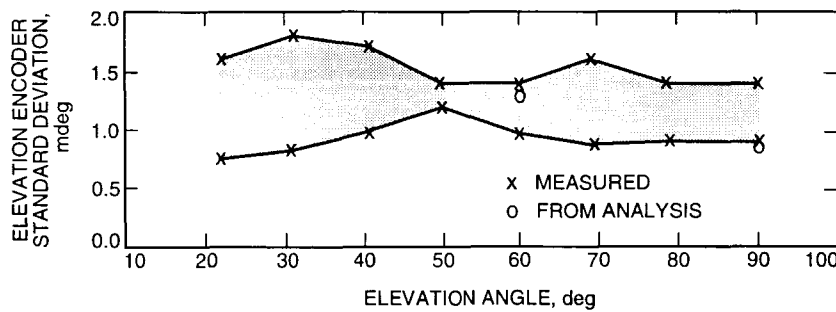


Fig. 1. Standard deviation of the elevation encoder output due to 40-km/h wind front gusts.
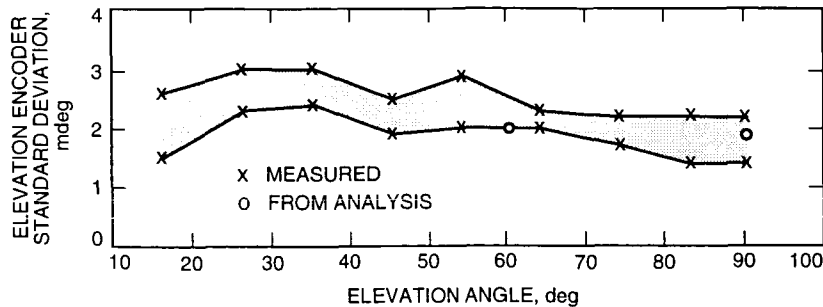


Fig. 2. Standard deviation of the elevation encoder output due to 40-km/h wind side gusts.
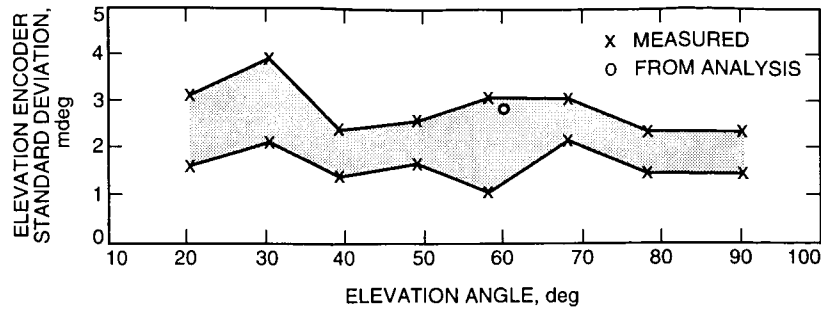
**Fig. 3. Standard deviation of the elevation encoder output due to 40-km/h wind back gusts.**
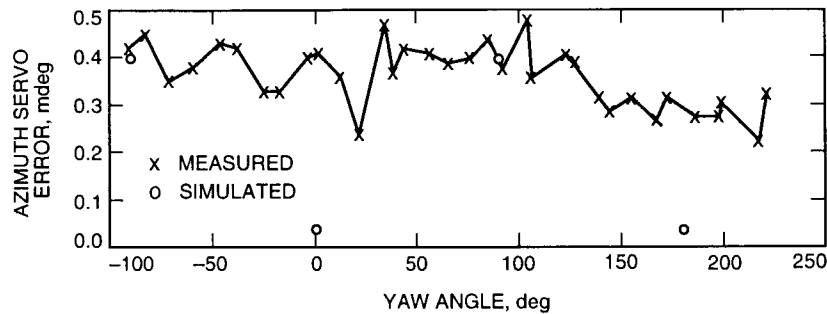


**Fig. 4. Standard deviation of the elevation encoder output due to 32-km/h wind gusts.**

and the coherence of the wind loading model. In reality, wind gusting is significantly unsymmetrical and is spatially uncorrelated. This discrepancy can be corrected by introducing an incoherent wind model using cross-spectra (see [5]).

## III. Wind Gust Model Derived From the Field Data

LQG controllers developed for the DSN antennas (see [4]) are based on the antenna model obtained from the field testing rather than on its analytical model. In order to evaluate the controller wind disturbance rejection properties as well as to improve these properties, one has to develop a wind disturbance model compatible with the antenna-identified model.

The antenna rate-loop model was identified for the azimuth and elevation loops separately. The cross-coupling between the azimuth and elevation axes, and vice versa, was low and was, therefore, ignored. The input to the model is the rate command, and the output is the encoder reading. The rate command creates difficulties in implementation of the analytical wind gust model because the wind is modeled as pressure at the antenna structure and is not readily transformed into the rate command disturbance, but this can be done by using the measured servo errors due to the wind gust disturbance.

Further, only the antenna model in azimuth is considered (the elevation model is developed similarly). The filter at the rate input will model the wind gusts (see Fig. 5). The white noise disturbance, $w(t)$, of unit intensity at the input to the wind filter is assumed. The filter transfer function, $G(s)$, is to be determined. The filter output, $w_r(t)$, adds to the rate command, and it serves as the wind gust model.
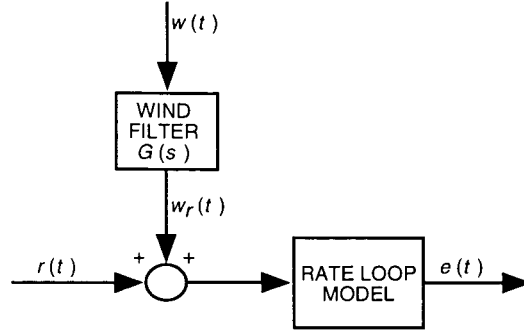
**Fig. 5. Wind filter configuration.**

Let the servo error due to the wind gusts be $e(t)$ and its spectrum be $e(\omega)$. The servo error due to disturbance $w(t)$ is $e_s(t)$, and its spectrum is $e_s(\omega)$. The filter transfer function, $G(\omega)$, is determined such that the difference between the simulated and the measured power spectrum is minimized as follows:

$$G(\omega) \text{ such that } \| e(\omega) - e_s(\omega) \| \text{ is minimal} \tag{1}$$

The filter that satisfies Condition (1) is called the wind filter.

Let $G_r(\omega)$ be the antenna rate-loop transfer function from the rate input to the encoder servo error. Then the simulated error due to wind gusts is obtained as

$$e_s(\omega) = G_r(\omega)G(\omega)w(\omega) \tag{2}$$

In Eq. (2), the spectrum $w(\omega)$ is constant (independent of frequency), and the transfer function $G_r(\omega)$ is dominated by the antenna resonance frequencies. In this case, the magnitude of the filter transfer function can be assumed to be a smooth curve in the form of a shaped integrator, that is,

$$G(s) = \frac{k}{s} \frac{(T_1 s + 1)^2}{(T_2 s + 1)(T_3 s + 1)^2} \tag{3a}$$

where the time constants are

$$
\left.
\begin{aligned}
T_1 &= \frac{1}{2\pi f_1} \\[2ex]
T_2 &= \frac{1}{2\pi f_2} \\[2ex]
T_3 &= \frac{1}{2\pi f_3}
\end{aligned}
\right\} \tag{3b}
$$

and $f_1 = 2.2$ Hz, $f_2 = 7.0$ Hz, and $f_3 = 12.0$ Hz are the frequencies where the magnitude of the integrator $k/s$ is shaped. The frequencies $f_1$ and $f_2$ determine the bandwidth of resonance frequencies of the antenna, and the frequency $f_3$ is the cut-off frequency for the wind disturbances. In this transfer function, the only unknown parameter is the gain, $k$. The plot of $G(\omega)$ is shown in Fig. 6 for $k = 1$. The
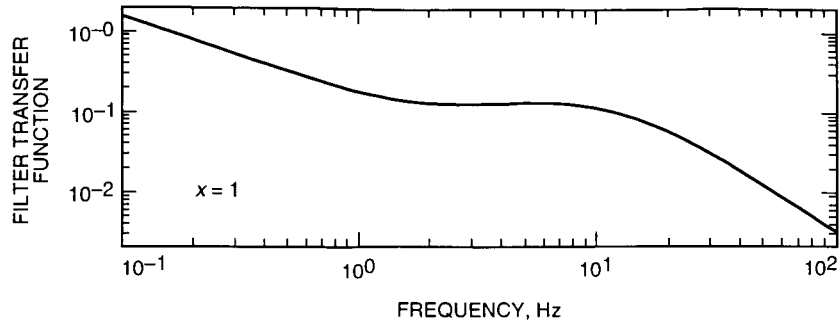
**Fig. 6. Magnitude of the wind filter transfer function for $k = 1$.**

choice of the transfer function shape as in Eq. (3) was done after the investigation of the more general case, where $G(s)$ was a rational function of polynomials of order 5 or less. The performance errors for the polynomials were almost the same as for $G(s)$ in Eq. (3).

The wind model for the azimuth rate loop was determined for two antenna elevation positions: 60 and 11 deg. For each elevation position, the wind from the front, side, and back was considered. The spectra of the azimuth encoder output, measured and simulated, are shown in Fig. 7 for an elevation angle of 60 deg and a wind direction from the back of the antenna. The measured spectrum shows two resonances, at 1.7 and 4.2 Hz, and the spectrum from simulations has an additional resonance peak at 3.1 Hz. The spectra are coincidental at the first three frequencies. The time series of measured and simulated encoder outputs are shown in Figs. 8(a) and 8(b), respectively. They show the similarity; the difference between their standard deviations was less than 7 percent. The gain, $k$, in this case was 0.0095.
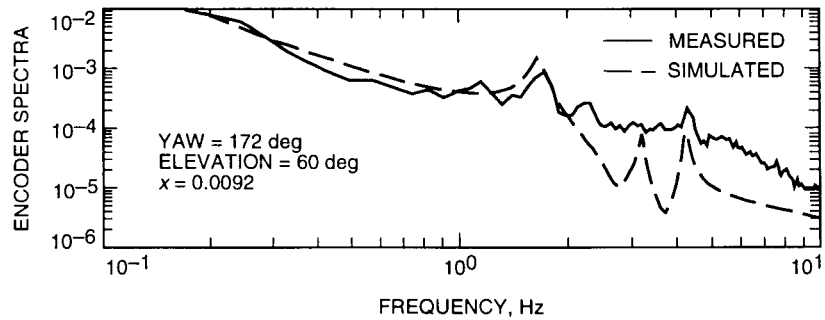


**Fig. 7. Azimuth encoder spectra.**

Similar results were obtained for other cases. Gain $k$ for an 11-deg elevation angle was as follows:

| Front wind | Side wind | Back wind |
|------------|-----------|-----------|
| 0.0075 | 0.0079 | 0.0075 |

Gain $k$ for a 60-deg elevation angle was as follows:

34

| Front wind | Side wind | Back wind |
| --- | --- | --- |
| 0.0095 | 0.0096 | 0.0092 |

The tables show that for a given elevation angle the gains for front, back, and side winds are almost the same. Therefore, the wind filter is independent of wind direction; however, it depends on the antenna elevation angle.
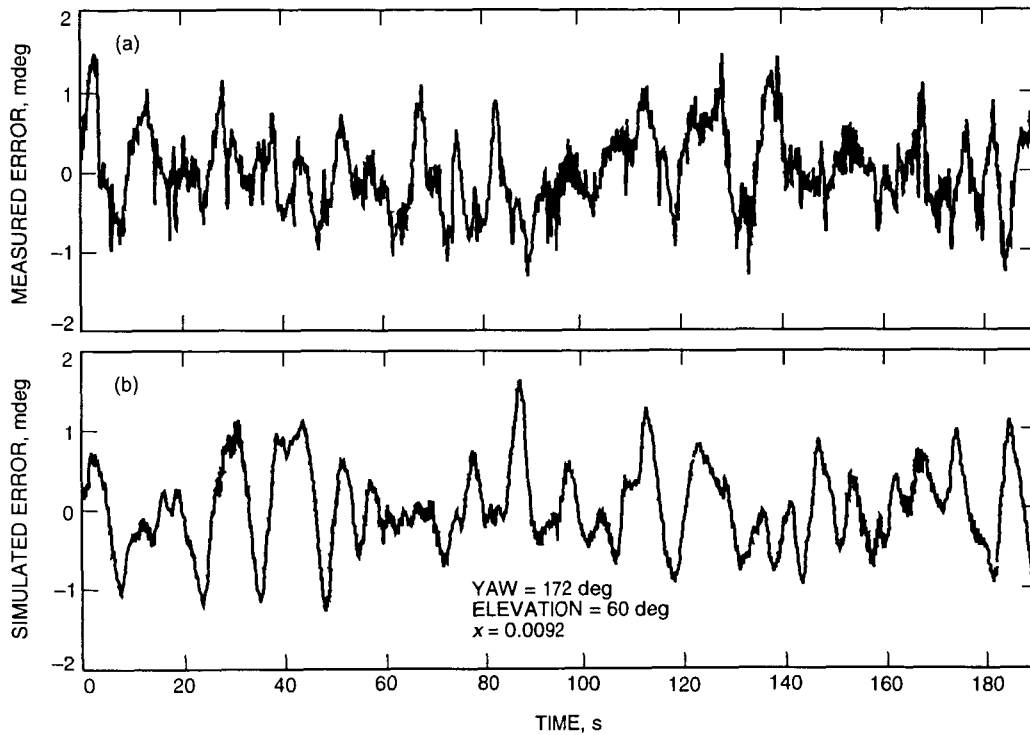


Fig. 8.  Azimuth encoder error due to 32-km/h wind gusts from the back at a 60-deg elevation angle:  (a) measured and (b) simulated.

## IV. Conclusions

The measured wind data at the DSS-13 site were used to verify the analytical wind model. The comparison showed that servo errors from the analytical model fall within the measured servo error boundaries. However, for the front and back winds, the simulated azimuth errors were smaller than the measured ones. This occurred because of the assumption of the spatial coherence of the wind gust model. The coherence caused a symmetric antenna load and, in consequence, a low azimuth servo error. This shortcoming indicates a need for upgrading the analytical wind model so that the spatially incoherent wind gust model reflects the real gusts in a more accurate manner.

The measured wind data were also used to generate a new wind model more suitable for the design of a control system with wind disturbance rejection properties. The wind filter was obtained for the antenna azimuth model for different elevation angles and different wind directions such that the simulated servo error is close to the measured one.

# References

[1] W. Gawronski, B. Bienkiewicz, and R. E. Hill, "Wind-Induced Dynamics of a Deep Space Network Antenna, *Journal of Sound and Vibration*, vol. 174, no. 5, pp. 67–77, 1994.

[2] W. Gawronski and J. A. Mellstrom, "Field Verification of the Wind Tunnel Coefficients," *The Telecommunications and Data Acquisition Progress Report 42-119, July–September 1994*, Jet Propulsion Laboratory, Pasadena, California, pp. 210–220, November 15, 1994, URL http://edms-www.jpl.nasa.gov/tda/progress_report/42-119/119G.pdf.

[3] C. S. Racho and W. Gawronski, "Experimental Modification and Identification of the DSS-13 Antenna Control System," *The Telecommunications and Data Acquisition Progress Report 42-115, July–September 1993*, Jet Propulsion Laboratory, Pasadena, California, pp. 42–53, November 15, 1993.

[4] W. Gawronski, C. S. Racho, and J .A. Mellstrom, "Linear Quadratic Gaussian and Feedforward Controllers for the DSS-13 Antenna," *The Telecommunications and Data Acquisition Progress Report 42-118, April–June 1994*, Jet Propulsion Laboratory, Pasadena, California, pp. 37–55, August 15, 1994, URL http://edms.jpl.nasa.gov/tda/progress_report/42-118/118D.pdf.

[5] E. Simiu and R. H. Scanlan, *Wind Effects on Structures*, New York: Wiley–Interscience, 1978.